frontiers | Frontiers in Earth Science

TYPE Original Research
PUBLISHED 10 May 2023
DOI 10.3389/feart.2023.1185964

Check for updates

OPEN ACCESS

EDITED BY
Shihua Zhong,
Ocean University of China, China

REVIEWED BY
Changhao Li,
Institute of Geology and Geophysics, Chinese Academy of Sciences (CAS), China
Guang Wen,
China University of Geosciences Wuhan, China

*CORRESPONDENCE
Li-Chuan Pan,
panlichuan@mail.gyig.ac.cn

RECEIVED 14 March 2023
ACCEPTED 21 April 2023
PUBLISHED 10 May 2023

CITATION
Liu Q, Pan L-C, Wang X-S, Yan J and Xing L-Z (2023), Apatite geochemistry as a proxy for porphyry-skarn Cu genesis: a case study from the Sanjiang region of SW China.
Front. Earth Sci. 11:1185964.
doi: 10.3389/feart.2023.1185964

Apatite geochemistry as a proxy for porphyry-skarn Cu genesis: a case study from the Sanjiang region of SW China

Qian Liu[1,2], Li-Chuan Pan[1]*, Xin-Song Wang[1], Jun Yan[1] and Lang-Zhang Xing[1]

[1]State Key Laboratory of Ore Deposit Geochemistry, Institute of Geochemistry, Chinese Academy of Sciences, Guiyang, China, [2]College of Earth and Planetary Sciences, University of Chinese Academy of Sciences, Beijing, China

In view of the importance of the magmatic oxidation state and volatile composition (H_2O-S-Cl) in porphyry Cu mineralization, identification of magmatic information has become the basis for the evaluation of the Cu-mineralization potential of porphyries. Apatite, as a common accessory mineral in porphyry, is recognized as an effective petrogenetic and metallogenic indicator. In this study, we analyze the *in situ* major and trace elements and Nd isotope content of apatite from four granitic plutons in the Yidun Terrane, SW China, in order to provide new insights into the identification of the magmatic features of Cu-mineralized plutons. The plutons investigated in this study are a Cu-mineralized pluton (Hongshan) and three non-mineralized plutons (Cilincuo, Rongyicuo, and Hagela). Chemical composition and textural analysis indicate that the apatites are all of magmatic origin and have not been altered. Our results show that apatite δCe values rather than δEu and Ga values are more valid indicators of the magma oxidation state of the four plutons. Based on apatite δCe values and zircon compositions, the parental magma of the Hongshan pluton is identified as having been more oxidized than those of the other three plutons. Moreover, the higher Cl content (0.06–0.23 wt%) in the Hongshan apatite compared to that in apatite from the other three plutons (0.01–0.09 wt%), indicates that the parental magma of the former pluton was more enriched in Cl. Apatite from the Hongshan pluton contains more SO_3 (average 0.05 wt%) than that from the other three plutons (SO_3 content mostly lower than the detection limit of electron probe micro-analysis), which may be related to higher magmatic oxygen fugacity of the Hongshan pluton. In addition, the Nd isotopic composition of apatite [$\varepsilon_{Nd}(t)$: −13.6–5.9] demonstrates that the Cu-mineralized and non-mineralized plutons were derived from the melting of ancient lower crust. Furthermore, based on the geochemical signature of adakite revealed by apatite Sr/Y and δEu values, the Hongshan pluton can be considered to have been produced as the result of partial melting of the thickened lower crust. Finally, an index system consisting of apatite δCe, Sr/Y, and F/Cl values is established to distinguish between the Cu-mineralized and non-mineralized plutons.

KEYWORDS

apatite, porphyry Cu deposit, magma oxidation state, volatile, the yidun terrane

1 Introduction

Porphyry Cu deposit is the most important reservoir of Cu globally (Sillitoe, 2010). Numerous studies have shown that oxidized and water-rich and sulfur-chlorine rich granitoid magmas are favorable for porphyry Cu mineralization for several reasons (Mungall, 2002; Richards, 2003; Sillitoe, 2010; Wang P et al., 2018; Wang et al., 2020). Firstly, magmas rich in water can exsolve sufficient hydrothermal fluids (Richards, 2003; Wang et al., 2014b; Cooke, 2014; Hou et al., 2015; Lu et al., 2015). Secondly, high oxygen fugacity avoids the loss of S in the melt caused by sulfide crystallization and ensures that most S can dissolve in melts in the form of S^{6+} (Steck and Dilles, 1998; Jugo et al., 2001; Richard, 2015). Additionally, Cl and S can participate in the migration and precipitation of Cu during magma related and hydrothermal processes (Webster, 2004). Therefore, identifying magmatic characteristics of a porphyry is the key to the evaluation of its Cu mineralization potential. However, due to weathering and hydrothermal alteration, whole-rock geochemistry may not be an effective tool for investigating the original physical and chemical natures of magmas. By contrast, accessory minerals, such as apatite and zircon have gradually become recognized as more useful petrogenetic and metallogenic indicators because of their abundant trace elements and resistance to post-magmatic reformation (Pan et al., 2016; Chelle-Michou and Chiaradia, 2017; Laurent et al., 2017; Richards et al., 2017; Konecke et al., 2019; Sun et al., 2019; Nathwani et al., 2020; Tang et al., 2020; Wen et al., 2020; Xing et al., 2020; Wang et al., 2021; Xing et al., 2021; Zhou et al., 2022a; Zhou et al., 2022b).

Apatite [$Ca_5(PO_4)_3F$] as an important accessory mineral, is widespread in granitic porphyry. Apatite is relatively stable and rich in trace elements and volatile components, which makes it capable of recording a large array of magmatic information during apatite crystallization (Zhao, 2010; Miles et al., 2014; Bruand et al., 2016). Previous studies have confirmed that variations in the chemical composition of apatite are closely related to magmatic physical and chemical natures. Specifically, apatite δEu, Mn, Fe, U, SO_3, and V values can vary with the change of magmatic oxygen fugacity (Candela, 1986; Martin and John, 1998; Chappell, 1999; Jeffrey and Scott, 1999; Piccoli and Candela, 2002). Apatite Cl, F, and S content are indicative of magmatic volatile composition (Martin and John, 1998; Piccoli and Candela, 2002) and the variation of apatite Sr, Y, and REE can reflect magmatic evolution (Pan et al., 2016). Additionally, apatite Sr and Nd isotopes can be used to trace magma sources (Creaser and Gray, 1992; Tsuboi and Suzuki, 2003; Tsuboi, 2005; Zhang et al., 2011).

In this study, we investigate the major and trace elemental concentrations and Nd isopote composition of apatite from four late Cretaceous granitic plutons located on the Yidun Terrane, southwestern China, i.e.,: the Cu-mineralized Hongshan pluton, and the non Cu-mineralized Cilincuo, Rongyicuo and Hagela plutons. Our results, based on differences in apatite chemical composition between the four plutons, indicate that the Cu-mineralized magma (Hongshan) is more oxidized and contains more Cl than the non-mineralized magmas (Rongyicuo, Hagela, and Cilincuo). Apatite Nd isotope, Sr/Y and δEu values suggest that the Hongshan pluton was mainly derived from partial melting of the thickened lower ancient crust. Moreover, we establish an index system consisting of apatite δCe, Sr/Y, and F/Cl values to distinguish Cu-mineralized and non-mineralized granite plutons. Overall, our study provides a new method for the identification of physical and chemical natures of magmas associated with porphyry Cu mineralization using the chemical composition of apatite.

2 Geological background and samples

The Yidun Terrane, as an integral component of the Sanjiang Tethys tectonic belt and is situated between the Jinsha River suture zone and the Ganzi-Litang suture zone (Wang et al., 2014a; Chen et al., 2017; Wang R et al., 2018) (Figure 1). The Yidun Terrane was formed by the massive westward subduction of the Ganzi-Litang ocean beneath the Zhongza-Zhongdain massif during the late Triassic. The ocean slab subduction and continental collision generated a sequence of late Triassic porphyry Cu deposits in the Southern Yidun Terrane, including the Pulang, Xuejiping, Lannitang and Chundu deposits (Li et al., 2011; Deng et al., 2014; Deng et al., 2016; Deng et al., 2017). After the collision of the Zhongza-Zhongdian massif and Songpan-Ganzi block, the regional tectonic regime began to transition from squeeze to extension. In the late Cretaceous, the strike-slip extension induced by the collision of the Lhasa and the Qiangtang block triggered the intracontinental magmatism in the Yidun Terrane (Hou et al., 2007; Li, 2010; Mao et al., 2012; Qing et al., 2014; Deng et al., 2016). The granitic plutons formed by the late Cretaceous magmatism produced several porphyry-skarn Cu ± Mo deposits in the southern Yidun Terrane including the Hongshan, Tongchanggou and Relin deposits, while the coeval plutons in northern Yidun Terrane are generally Cu-infertile.

The Hongshan pluton, which is located in the southern Yidun Terrane, consists of early Permian and late Cretaceous granitic plutons and hosts a typical porphyry-skarn Cu deposit (Figure 2A). The consistency between zircon U-Pb ages (81.1 ± 0.5 Ma) and molybdenite Re-Os ages (81.2 ± 2.6 Ma) imply that the late Cretaceous pluton has potential genesis relationship with porphyry-skarn Cu mineralization (Wang et al., 2011). The late Cretaceous granitic plutons are mainly composed of quartz monzonite porphyry. In this study, four quartz monzonite porphyry samples from the Hongshan plutons were collected. The quartz monzonite porphyry is grey and coarse grained. The main rock-forming minerals are K-feldspar, plagioclase, quartz, biotite, and amphibole. Accessory minerals are apatite, zircon, and titanite. Previous studies on the fluid inclusions, H-O isotope and S-Pb-Re isotope of sulphide have shown that the ore-forming fluid of the Hongshan deposit is mainly magmatic fluid and the ore-forming elements are mainly derived from magma (Wang et al., 2014a). The above chemical evidence confirms the genetic relationship between the porphyry-skarn Cu deposit and the quartz monzonite porphyry.

The Cilincuo, Rongyicuo, and Hagela plutons are located in the northern Yidun Terrane and do not produce any important porphyry Cu mineralization. The Cilincuo pluton is composed of biotite granite and a small volume of fine-grained monzogranite (Figure 2B). The zircon U-Pb age of the Cilincuo pluton is 86.1 ± 0.5 Ma (Pan et al., 2021). In this study, two biotite granite samples from the Cilincuo plutons were collected. The biotite granite is grayish-white and coarse-medium grained. Major rock-forming minerals are K-feldspar, plagioclase, quartz, biotite, and amphibole. The accessory minerals are zircon, titanite, and apatite. The Rongyicuo pluton is dominated by monzogranite (Figure 2B) with a zircon U-Pb age of 98.0 ± 0.5 Ma

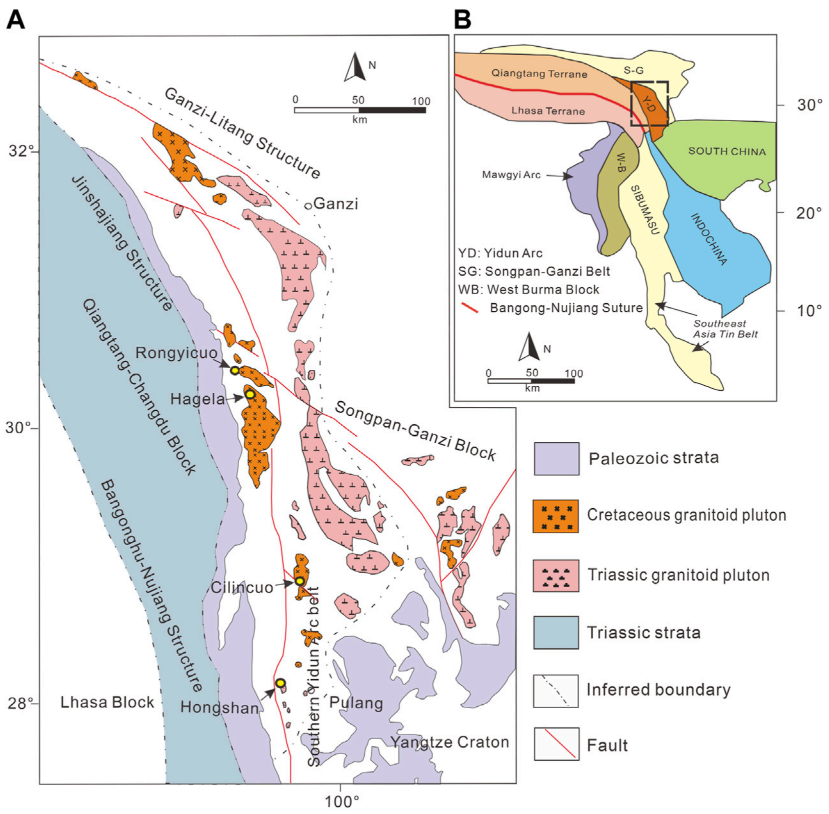

FIGURE 1
(A) Tectonic framework of the Yidun arc (modified after Hou et al., 2007; Wang et al., 2014a; Yang et al., 2014).**(B)** Regional location map showing terranes accreted in the Late Palaeozoic, in part based on previous studies (Schwartz et al., 1995; Metcalfe, 2011; Zhu et al., 2011; Morley, 2012; Zhang et al., 2012).

(Pan et al., 2021). Four monzogranite samples from the Rongyicuo plutons were selected for study. The rock samples contain quartz, plagioclase, K-feldspar, and biotite as major phases, and apatite, allanite, and zircon as accessory phases. The main lithofacies of the Hagela pluton is monzogranite (Figure 2C) with a zircon U-Pb age of 97.1 ± 0.8 (Pan et al., 2021). Three monzogranite samples from the Hagela pluton were selected for study. Similar to the Rongyicuo monzogranite, the Hagela monzogranite mainly consists of quartz, plagioclase, K-feldspar, and biotite. Accessory phases include apatite and zircon.

Apatite is widespread in the above four plutons. The apatites from the Cu-mineralized Hongshan pluton are mainly transparent short columnar-fine hexagonal grains with 120–150 μm in length and 50–60 in width. The apatites, as euhedral grains, are usually wrapped by plagioclase, quartz and biotite. The apatites from the non-mineralized Cilincuo, Rongyicuo and Hagela plutons are mainly transparent short columnar euhedral-subhedral grains with 80–120 μm in length and 50–70 in width. The apatites are mainly wrapped by K-feldspar, plagioclase, amphibole quartz, and biotite.

3 Analysis methods

3.1 Whole-rock compositions

The whole rock samples used in this study were relatively fresh and did not show obvious Cu mineralization. An Axios PW4400 X-ray fluorescence spectrometer was used to determine the concentrations of the major elements in the selected rocks using fused tetraborate glass pellets in the State Key Laboratory of Deposit Geochemistry (SKLODG), Institute of Geochemistry, Guiyang Chinese Academy of Sciences. Analysis uncertainty was estimated to be less than ±5%.

Concentrations of trace elements in the whole rock were analyzed using PE DRC-e ICP-MS in SKLODG. A powder sample (50 mg) was dissolved in a high pressure PTFE vessel at 190°C for 2 days using a mixture of HF and HNO_3. During the analysis, Rh was used to monitor signal drift. Qi et al. (2000) give full details of the analysis methods. The analysis uncertainty was estimated to be within ±10%.

3.2 Apatite main and trace element compositions

Apatite crystals were separated from rock samples using standard heavy liquid and magnetic methods and then mounted and polished in epoxy. Targets suitable for *in situ* analysis were chosen to produce cathodoluminescence (CL) images. The CL images showed that the surfaces of the apatite grains were clean and without cracks, which suggests that the apatite had not been altered and the apatite could be used to validly record the original magma information.

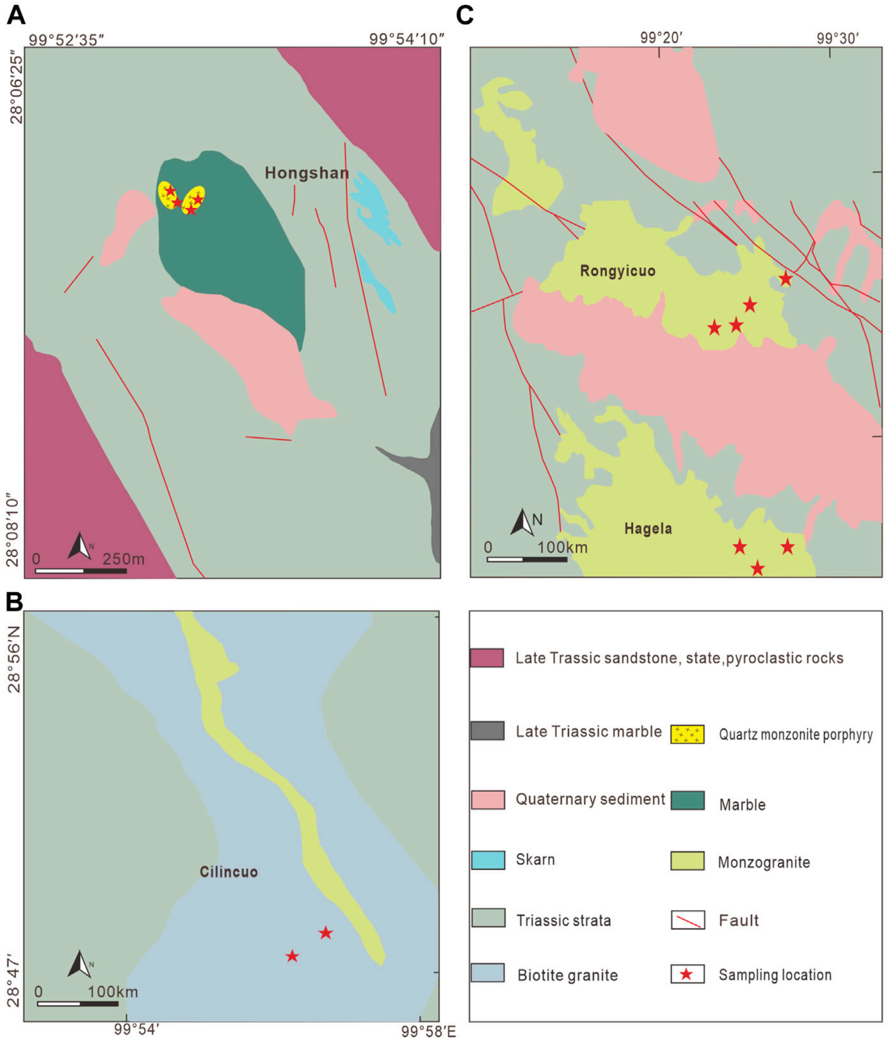

FIGURE 2
Simplified geological maps of **(A)** the Hongshan, **(B)** Cinlincuo, and **(C)** Rongyicuo, and Hagela plutons (modified after Wang et al., 2014a; Peng, 2014).

The contents of major and minor elements in the apatite were determined using a JXA8530F-plus electron microprobe at SKLODG. The analysis conditions were: 25 KV accelerating voltage, 10 na beam current and 10 μm beam diameter. The direction of the electron beam was perpendicular to the apatite caxis to minimize the error of the F analysis (Stormer et al., 1993; Goldoff et al., 2012). The following natural minerals were used for calibration: Apatite (P, S, and F), kaersutite (Ca, Mn, Na, Al, Si, and Fe), and tugtupite (Cl). The concentrations of trace elements in the apatite was measured by field LA-ICP-MS in the SKLODG. The LA-ICP-MS system was an Agilent 7500a ICP-MS, equipped with M-50 resolution ArF excimer laser gun (λ = 193 nm, 80 mJ, and 10 Hz). The laser ablation spot diameter was 44 μm. Aerosol after ablation was sent into an ICP instrument with helium. NIST610 and NIST612 standards were used for calibration. The content of Ca was measured using ^{43}Ca and normalized using the concentration determined by electron probe analysis. Off-line data reduction was then performed using the ICPMSDataCal software from Liu et al. (2008).

3.3 Apatite Nd isotopes

The *in situ* apatite Nd isotope measurements were conducted on an Nu Plasma III MC-ICP-MS (Nu Instruments) equipped with a RESOlution-155 ArF193-nm laser ablation system (Australian Scientific Instruments) at SKLODG. The interference of ^{144}Sm on ^{144}Nd originates from ^{147}Sm intensity, and the natural ratio of ^{144}Sm/^{147}Sm is 0.205484 (Isnard et al., 2005). The mass deviation coefficient of Sm was calculated according to the measured ^{147}Sm/^{149}Sm isotope ratio and its actual value of 1.08680 (Isnard et al., 2005). The mass deviation of ^{143}Nd/^{144}Nd was normalized to ^{146}Nd/^{144}Nd = 0.7129. One apatite standard (Durango) was analyzed for every five samples, and the other two apatite standards (AP1 and MAD) were analyzed for every thirty samples. The results were used for quality control. The ^{143}Nd/^{144}Nd ratio of apatite standard AP1 was 0.512493 ± 0.000040 (n = 9), which was the same as the

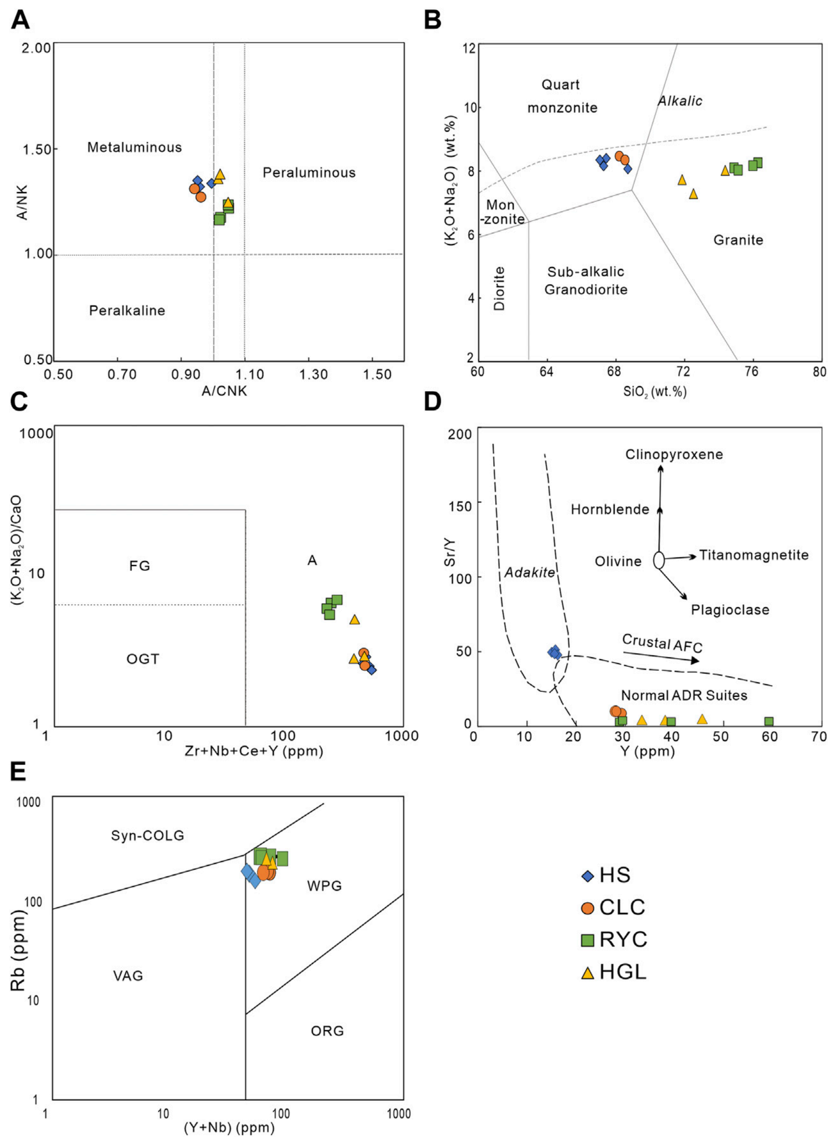

FIGURE 3
(A) A/NK vs. A/CNK diagram (Piccoli, 1989). **(B)** Total alkali vs. SiO_2 diagram (Middlemost, 1994). **(C)** K_2O+ Na_2O)/CaO vs. Zr+Nb+Ce+Y diagram (Whalen et al., 1987). **(D)** Sr/Y versus Y classification diagram for identifying adakitic rocks (Defant and Drummond, 1990). **(E)** The Rb-(Y+Nb) diagram for discriminating the tectonic setting of granites (from Pearce et al., 1996). Date are listed in Supplementary Appendix Table SA1. HS, Hongshan; CLC, Cilincuo; RYC, Rongyicuo; HGL, Hagela.

recommended value (AP1: 0.512352 ± 0.000024) (Yang et al., 2014).

3.4 Zircon trace elements compositions

Trace elements in zircon from the Hongshan pluton were determined by LA-ICP-MS at the above-mentioned laboratory. Zircon was sampled using a GeoLasPro laser-ablation system. Ion-signal intensities were acquired using an Agilent 7500a ICP-MS instrument with helium (He) as the carrier gas. The ablation protocol employed a spot diameter of 44 mm at a 4 Hz repetition rate. The NIST610 and NIST612 standards were used for calibration. Off-line data reduction was then performed using the ICPMSDataCal software from Liu et al. (2008).

4 Results

4.1 Whole-rock compositions

The whole-rock major and trace elemental contents of the four plutons are presented in the Supplementary Appendix Table SA1. The results show that the SiO_2 content is 67.06–68.69 wt% in the Honshan pluton, 68.19–68.52 wt% in the Cilincuo pluton, 74.87–76.26 wt% in the Rongyicuo pluton and 71.85–74.36 wt% in the Hagela pluton. The K_2O content is 4.11–4.43 wt% in the Honshan pluton, 4.69 wt% in the Cilincuo pluton, 4.83–5.04 wt% in the Rongyicuo pluton and 4.23–5.04 wt% in the Hagela pluton. Compared with the Rongyicuo pluton (3.14–3.22 wt%) and Hagela pluton (2.98–3.06 wt%), the Hongshan (3.85–3.99 wt%) and

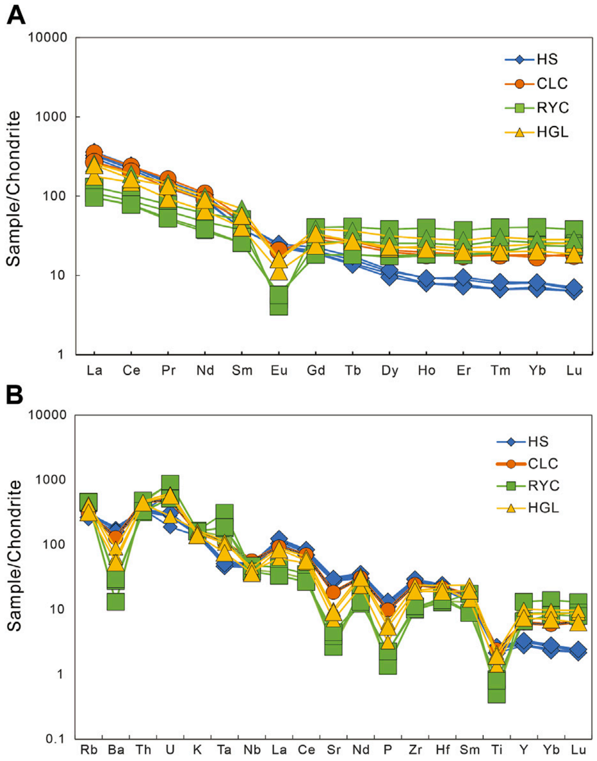

FIGURE 4
(A) Chondrite-normalized REE diagrams and **(B)** trace-element diagrams for the Hongshan, Cilincuo, Rongyicuo, and Hagela plutons. Date are listed in Supplementary Appendix Table SA1. The chondrite values are from Sun and McDonough (1989). HS:Hongshan, CLC, Cilincuo; RYC, Rongyicuo; HGL, Hagela.

Cilincuo (3.66–3.78 wt%) plutons have higher Na_2O content. The content of Fe_2O_3 in the Hongshan pluton (2.95–3.66 wt%) and Cilincuo pluton (3.25–3.48 wt%) is slightly higher than that in the Rongyicuo pluton (1.33–1.76 wt%) and the Hagela pluton (2.18–3.15 wt%).

The Rittmann index (1.93–3.16) and the aluminum saturation index (0.94–1.05) indicate that the four plutons are classified as calc-alkaline and metaluminous–weakly peraluminous granite (Figures 3A, B). Due to the high content of high field-strength elements, the four plutons belong to A-type granite (Figure 3C). The Hongshan pluton exhibits geochemical characteristics similar to adakite (high Sr/Y:41.9–45.7, $(La/Yb)_N$: 42.3–45.7, and δEu: 0.78–0.85), while the other three plutons do not (Figure 3D). In the discriminant diagram of the granite-related tectonic background (Pearce 1996), all of the rock samples fall within the field of within-plate granite (Figure 3E). Combined with regional tectonic evolution history between 98 Ma to 85 Ma (Wang et al., 2014a; Li et al., 2021), we can conclude that the four plutons were formed in an intra-continental extensional setting without ocean slab subduction.

In the chondrite-normalized REE diagram (Figure 4A), all the samples display fractionated REE patterns. The $(La/Yb)_N$ value is highest in the Hongshan pluton (42.3–45.7), medium in the Cilincuo pluton (15.8–19.32) and the Hagela pluton (7.19–12.16), and lowest in the Rongyicuo pluton (3.22–4.23). The δEu value is highest in the Hongshan pluton (0.78–0.85), medium in the Cilincuo pluton (0.48–0.54) and the Hagela pluton (0.31–0.37), and lowest in the Rongyicuo pluton (0.09–0.28). In primitive mantle-normalized trace elements spider diagrams (Figure 4B), all rock samples show Ba, Sr, P, and Ti depletion.

4.2 Apatite major and trace elements compositions

Analysis results of the apatite major and trace elements are presented in Supplementary Appendix Table SA2. The results show a limited variation of CaO, P_2O_5, and FeO contents in the apatites from the four selected plutons (CaO: 53wt% to 56wt%, P_2O_5,: 39 wt % to 42 wt%, and FeO: <0.12 wt%). The apatites from the Hongshan pluton contain more SO_3 (0.02 wt% to 0.10 wt% average 0.05 wt%), F (2.99wt% to 3.53 wt% average 3.41 wt%) and Cl (0.06 wt% to 0.21 wt% average 0.16 wt%) than those from the Cilincuo (SO_3: Most are below the detection limit, F: 2.61 wt% to 3.08 wt% average 2.84 wt%, Cl: 0.04 wt% to 0.09 wt% average 0.07 wt%), Rongyicuo (SO_3: Most are below the detection limit, F: 2.70 wt% to 3.14 wt% average 2.93 wt%, Cl: 0.01 wt% to 0.02 wt% average 0.01 wt%) and Hagela (SO_3: Most are below the detection limit, F: 2.96 wt% to 3.40 wt% average 3.13 wt%, Cl:<0.03 wt% average 0.02 wt%) plutons.

The variation range of the total REE content of the apatite is 2087–16,229 ppm. The high LREE/HREE values (1.80–31.65) demonstrate the enrichment of LREE relative to HREE in all of the apatites. The apatites from the Hongshan pluton show more Eu negative anomalies than those from the Rongyicuo, Hagela and Cilincuo plutons, which is consistent with the feature of an Eu negative anomaly in host rocks. Apatite δCe value is highest in the Hagela pluton (1.12–1.19, average 1.16), medium in the Rongyicuo (1.12–1.14, average 1.13) and Cilincuo plutons (1.09–1.14, average 1.11), and lowest in the Hongshan pluton (1.06–1.15, average 1.09). The Cilincuo apatites have highest Ga content (14.18–43.70 ppm, average 20.95 ppm), the Hagela (13.63–28.50 ppm, average 16.39 ppm) and Hongshan apatites have medium Ga content (5.31–19.51 ppm, average 16.06 ppm) and the Rongyicuo apatites have lowest Ga content (9.30–13.33 ppm, average 11.76 ppm). The Hongshan apatites have the highest Sr content (335–764 ppm, average 550 ppm), the Cilincuo (141.54–366.46 ppm, average 188.77 ppm) and Rongyicuo (123.99–196.36 ppm, average 157.15 ppm) apatites have medium Sr content, and the Hagela apatites have lowest Sr content (103.99–178.67 ppm, average 122.08 ppm) (Figure 3).

4.3 Apatite Nd isotopes

The *in situ* Nd apatite isotope data are presented in Supplementary Appendix Table SA3. Based on the available zircon U-Pb ages (Wang R et al., 2014; Pan et al., 2021), we calculated the initial ε_{Nd} (t) values of apatite from the four plutons. The results show that the ε_{Nd} (t) values are −17.6 to −7.8 (average −13.6) in the Hongshan pluton, −18.3 to −6.7 (average −9.9) in the Cilincuo pluton, −19.2 to −3.7 (average −9.7) in the Rongyicuo pluton and −6.6 to −1.9 (average −4.9) in the Hagela pluton (Figure 5).

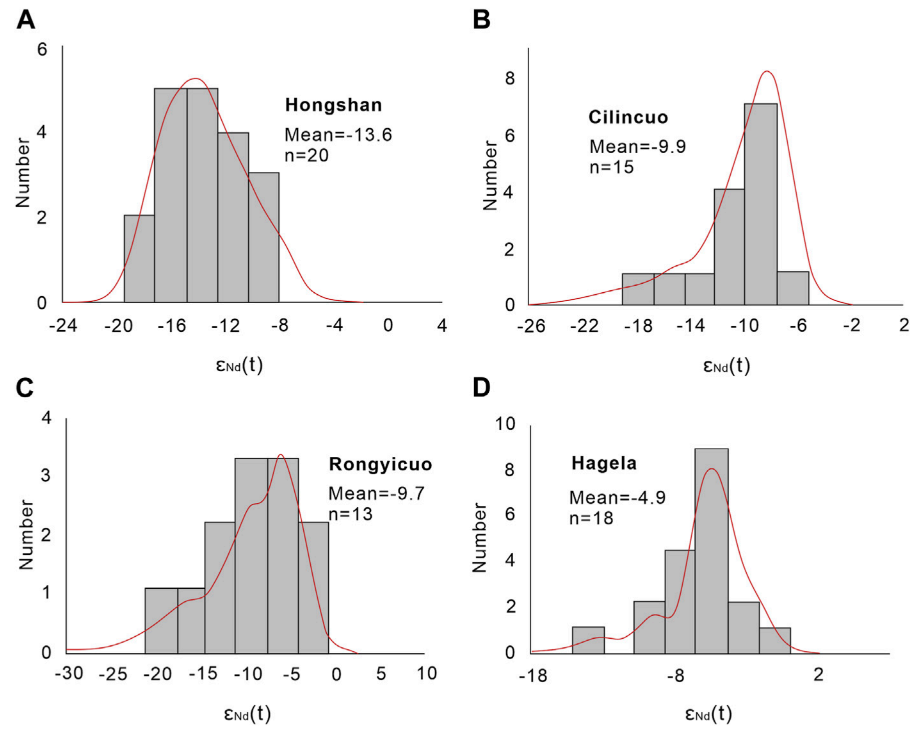

FIGURE 5
Probability density plot of apatite $\varepsilon_{Nd}(t)$ values in the Hongshan **(A)**, Cilincuo **(B)**, Rongyicuo **(C)** and Hagela **(D)**plutons. Date are listed in Supplementary Appendix Table SA3.

4.4 Zircon trace element compositions

The zircon trace-element contents of the Hongshan pluton are listed in Supplementary Appendix Table SA4. The average Ti, Ce, Th, and U contents of zircon are 4.85 ppm, 39.2 ppm, 622 ppm, and 1,158 ppm. Because of high Th/U ratios, the analyzed zircons are considered to be of magmatic origin (>0.1) (Moeller et al., 2003). We calculated magmatic oxygen fugacity of the Hongshan pluton using zircon chemical composition based on the method proposed by Louck et al. (2020). The result shows that magmatic oxygen fugacity value is ΔQFM =1.30 during zircon crystallization.

5 Discussion

5.1 Apatite origin

According to microscopic textural observation, apatites from the four plutons show euhedral morphology and are usually surrounded by biotite, quartz, and feldspar (Figure 6). This observation implies that apatite grains from the four plutons are of magma origin. However, because apatite analyzed in this study is separated from rocks, other evidence is needed to verify its genesis. Previous research (Piccoli and Candela, 2002) has shown that apatite crystallizing from hydrothermal fluids or subjected to hydrothermal alteration can have high Cl content (usually exceeding 3.0 wt%) because of the abundant Cl in the hydrothermal fluid. However, the apatite crystals chosen from the four plutons have relatively low Cl content (0.75 wt%). Moreover, the chemical compositions of the apatite analyzed, including Mn, Ca, Na, F, Cl, and H_2O (Figures 7A–C), are consistent with those in typical magmatic-origin apatite (Piccoli and Candela, 2002). In addition, the CL images of the apatite do not show obvious dissolution-reprecipitation textures (Figure 7D). Based on this evidence, it is concluded that the apatites in the four plutons are all of magmatic origin and did not undergo severe hydrothermal alteration. We calculated apatite saturation temperature using the equation proposed by Harrison and Watson (1984). The resulting high apatite saturation temperatures (993°C, 962°C, 872°C, and 943°C in the Hongshan Cilincuo, Rongyicuo, and Hagela plutons, respectively) indicate that the apatite from the four plutons may have crystallized early from magma.

5.2 Magmatic oxidation state

It has been generally accepted that the magma oxidation state plays a crucial role in the formation of porphyry Cu deposits (Richards, 2011; Wang et al., 2014b; Lu et al., 2016). Traditionally, whole-rock Fe^{3+}/Fe^{2+} ratio has been widely used to evaluate magma oxidation state. Our data shows that the Hongshan pluton has evidently higher whole-rock Fe^{3+}/Fe^{2+} ratios (0.37–0.54) than those of the Cilincuo, Rongyicuo and Hagela plutons (0.03–0.21), which implies that the former pluton was formed by a more oxidized magma system relative to other three plutons.

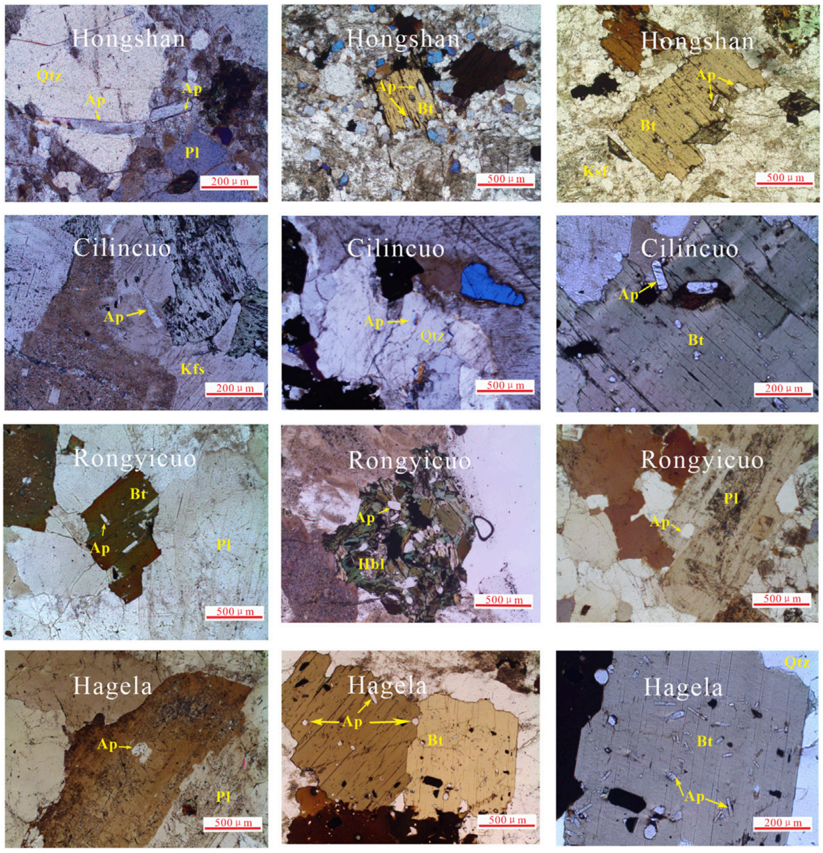

FIGURE 6
Modes of the occurrence of apatite in the rock samples from the selected plutons. Abbreviations Ap, apatite; Qtz, quartz; Pl, plagioclase; Bt, biotite, Ksf, K-feldspar; HBl, hornblende.

However, since weathering and alteration can change whole-rock Fe^{3+}/Fe^{2+}ratio, the oxidation state of the magma should be further evaluated using other indexes.

In recent years, many researchers have successfully used the composition of apatite to explore the magma oxidation state. Based on the sensitivity to magmatic oxygen fugacity change, apatite δEu, δCe, and Ga contents are considered as potential indicators for the magma oxidation state (Drake, 1975; Streck and Dilles, 1998; Sha and Chappell, 1999; Imai, 2002; Cao et al., 2012; Sun et al., 2019). Specifically, Ga^{3+}, Eu^{3+}, and Ce^{3+}, rather than Ga^{2+}, Eu^{2+}, and Ce^{4+}, can preferentially replace Ca^{2+} in apatite because their ionic radii are approximate to that of Ca^{2+} (Sha and Chappell, 1999). An increase in magmatic oxygen fugacity can lead to an increase in the contents of Ga^{3+}, Eu^{3+}, and Ce^{4+} in the melt by the conversion of Ga^{2+}, Eu^{2+}, and Ce^{3+} into Ga^{3+}, Eu^{3+}, and Ce^{4+}. Therefore, it is expected that apatite crystallizing in oxidized magma may have higher δEu values and Ga contents but lower δCe values than apatite crystallizing in less-oxidized magma if other factors such as magma composition and fractional crystallization have no significant influence on these values.

In this study, the apatite from the Hongshan pluton has much higher δEu values than those from the other three plutons, which probably indicates higher magmatic oxygen fugacity of the Hongshan pluton. However, it is observed that the whole-rock δEu value of the Hongshan pluton is also higher than those of the other three plutons. Thus, it is unclear whether the higher δEu value in the Hongshan apatite is caused by higher magmatic oxygen fugacity or inherits the characteristics of δEu from the magma. In addition, the positive correlation between apatite δEu value and Sr content (Figure 8A) implies that feldspar crystallization may have had an important effect on apatite δEu value. Similarly, the Hagela and Cilincuo plutons have higher whole-rock Ga content than the Hongshan and Rongyicuo plutons. The apatite from the former two plutons also contains more Ga than apatite from the latter two plutons. The consistent variation of Ga content between the apatite and its host rock suggests that the apatite Ga content may be largely determined by the magmatic Ga abundance.

Therefore, apatite δEu values and Ga contents may not be suitable indicators of the magma oxidation state for the four plutons. By comparison, the apatite δCe values may better reflect the difference in magma oxidation state of the four plutons because our data show that the whole-rock δCe values of the four plutons are approximate, but the apatite δCe value of the Hongshan is much lower than those of other three plutons. The observed decoupling between apatite δCe value and whole-rock δCe value implies that apatite δCe value may not be determined by the magmatic δCe value but more likely by the magma oxidation state. The lower apatite δCe value in the Hongshan pluton than those in other three plutons

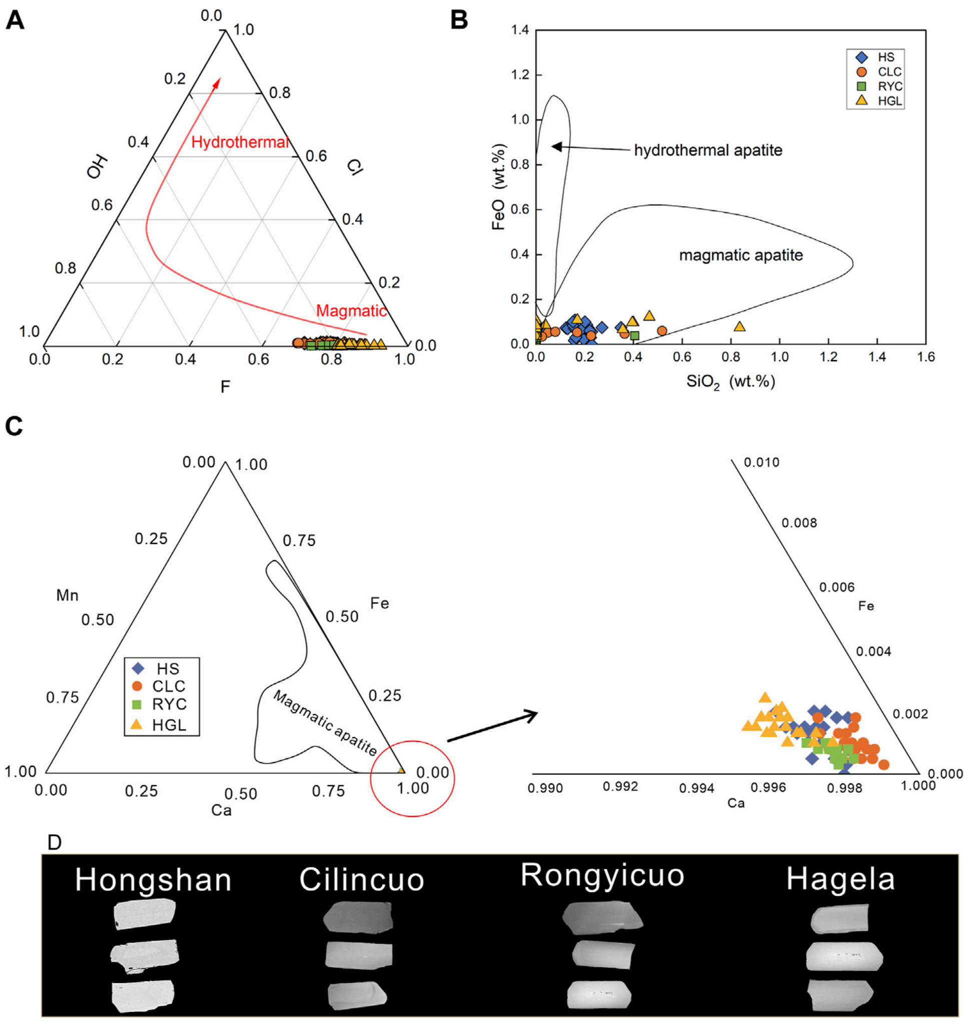

FIGURE 7
(A) Plots of F-Cl-OH variability in the halogen-site in apatite. The evolutionary line was cited from Palma et al., 2019. **(B)** Plots of apatite FeO versus SiO_2 from the four seleted plutons (Ketcham, 2015). **(C)** Plots of Mn-Fe-Ca variability from the apatite of four seleted plutons based on (Piccoli and Candela, 2002). **(D)** CL images of the representative apatite crystals from the four plutons for *in situ* analysis. HS: Hongshan; CLC, Cilincuo; RYC, Rongyicuo; HGL, Hagela (Date are listed in Supplementary Appendix Table SA2).

(Figure 8B) suggests that the parental magma of the Hongshan pluton was relatively oxidized. In addition, the calculated magma oxygen fugacity using zircon chemical composition based on the method proposed by Loucks et al. (2020) suggests that the magmatic oxygen fugacity of the Hongshan pluton is greater than ΔQFM+1 (Supplementary Appendix Table SA4). A previous study has suggested that the magmatic oxygen fugacity of the Cilincuo, Hagela, and Rongyicuo plutons is below ΔQFM (Pan et al., 2021). This evidence, consistent with the apatite δCe value and whole-rock Fe^{3+}/Fe^{2+} value, reinforces the idea that the Cu-mineralized magma (Hongshan) is more oxidized than the non-mineralized magma (Rongyicuo, Cilincuo, and Hagela).

5.3 Magmatic volatile components

During solidification of magma, volatiles including F, Cl, H_2O, and S are inevitably removed from the magma due to degassing. For hydrous magma (H_2O > 4 wt%), hydrothermal fluid saturation and exsolution can occur in the early stage of magmatic evolution (Zhu et al., 2018).

Since apatite is an early-crystallizing phase, which is revealed by the high apatite saturation temperature, apatite is a more valid tracer of volatile components of early-stage magma than hornblende and biotite which usually crystallize later than apatite.

The Cl and F abundances in the magmas were calculated using the apatite/melt partition coefficients of Parat et al. (2011). The results (Supplementary Appendix Table SA5) suggest that the parental magma of the Cu-mineralized Hongshan pluton contained more Cl (2000 ppm) than that of the non-mineralized Rongyicuo, Hagela and Cilincuo plutons (Cl: 200–800 ppm), whereas the magmatic F abundance of the above four plutons are consistent. In view of the important role of Cl in porphyry Cu mineralization, the high magmatic Cl content in the Hongshan pluton partly explains its elevated ore-forming ability relative to the other three plutons. Previous studies have shown that Cl exhibits a

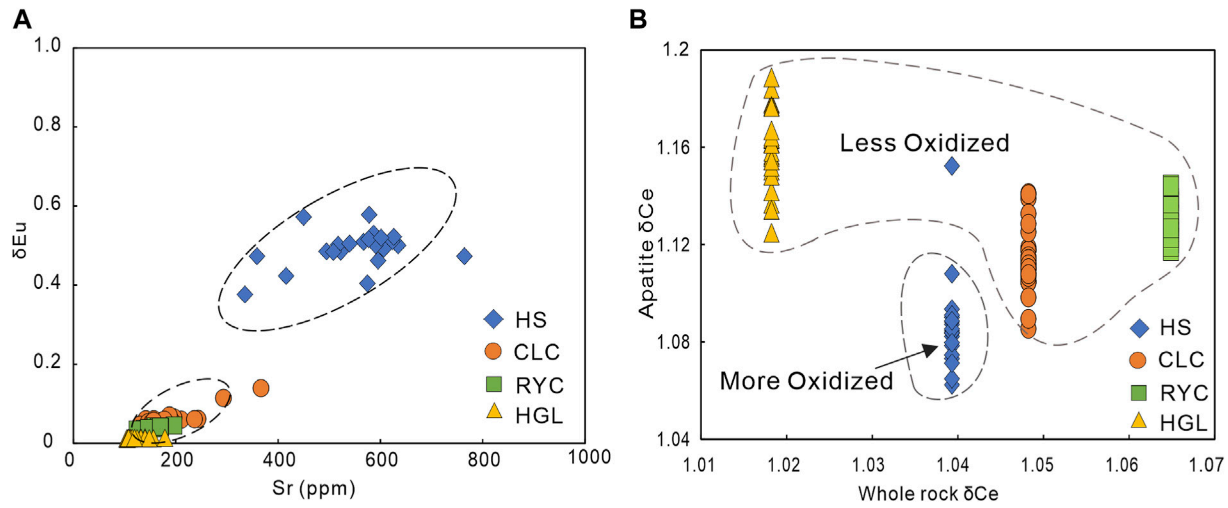

FIGURE 8
(A) Plots of δEu versus Sr, **(B)** Apatite δCe versus Whole rock δCe, and HS, Hongshan; CLC, Cilincuo; RYC, Rongyicuo; HGL, Hagela (Date are listed in Supplementary Appendix Tables SA1, 2).

strong preference for aqueous solutions relative to F (Candela, 1986; Boudreau and Kruger, 1990). It follows that hydrothermal fluid exsolution can lead to more loss of Cl rather than F in coexisting melts. Hence the increase in the F/Cl ratio of apatite may indicate continuous hydrothermal fluid exsolution during apatite crystallization (Huang et al., 2019). Considering that apatite is an early-crystallizing phase, the significantly changing F/Cl ratio of apatite from the Hongshan pluton may indicate that hydrothermal fluid exsolution can occur in the early stage of magmatic evolution. In fact, early exsolution of hydrothermal fluid is conducive to hydrothermal Cu mineralization because it can effectively avoid the loss of Cu caused by fractional crystallization.

Moreover, our data show that the Cu-mineralized Hongshan pluton has higher apatite SO_3 content than other three plutons. Previous studies have confirmed that the SO_3 content of apatite is largely affected by magma temperature and oxidation state (Peng et al., 1997; Parat et al., 2011; Chelle-Michou and Chiaradia, 2017; Richards et al., 2017; Huang et al., 2019). The consistent apatite saturation temperature of the four plutons, however, rules out temperature as being responsible for the difference in apatite SO_3 content. Thus, magmatic oxygen fugacity may play an important role in controlling the apatite SO_3 content of the four plutons investigated. As S^{6+} has an ionic radius simlar to that of P^{5+}, the elevated S^{6+} converted from S^{2-} in the melt caused by the increased magmatic oxygen fugacity can result in more S being incorporated by apatite. Considering that the causative magma of the Hongshan pluton was more oxidized than that of the Rongyicuo, Cilincuo, and Hagela plutons, the Hongshan apatite could thus incorporate more SO_3 than that from the other three plutons. It is noteworthy that comparing to apatites from other Cu-mineralized plutons with magmatic oxygen fugacity (△FQM >1) similar to the Hongshan pluton, such as the Qulong and Zhunuo plutons from the Tibetan Plateau (apatite SO_3 > 0.2 wt%) (Li et al., 2021), apatite from the Hongshan pluton contains much less SO_3 (<0.1 wt%). Therefore, the relatively low apatite SO_3 content of the Hongshan pluton may result from the low enrichment of S in its parental magma. The finding supports a popular view that the magma without extremely rich S can also have potential to form porphyry-skarn Cu mineralization (Xing et al., 2021).

5.4 Magma sources

Previous studies, based on whole-rock Sr-Nd and zircon Hf isotope data (Wang et al., 2014a; Pan et al., 2021), have concluded that the four plutons are the products of partial melting of ancient lower crust and mixed with a small amount of mantle-derived components. The evidently nagative $\varepsilon_{Nd}(t)$ values of the apatite (Supplementary Appendix Table SA3) also support an ancient lower crustal origin of the causative magmas of the four plutons. It is generally accepted that the collision-related porphyry Cu deposits are usually associated with intermediate-acid magmas derived from the partial melting of the juvenile lower crust characterized by $\varepsilon_{Nd}(t) \geq 0$, such as those in the Gangdese metallogenic belt (Hou et al., 2004; Guo et al., 2007; Hou et al., 2012). However, the genesis of the Cu-mineralized Hongshan pluton demonstrates that magma derived from the partial melting of the ancient lower crust may also have had the potential to form porphyry-skarn Cu deposits, especially when the magma had high oxygen fugacity and was rich in Cl, as revealed by the apatite chemical compositions presented in this study.

Based on the observed Sr/Y and δEu values of apatite (Figure 9), the Hongshan pluton is identified as adakite, while the other three plutons are not, which can be revealed by whole-rock chemical features as well (Figure 3D), Generally, adatikic geochemical features, such as high Sr/Y and δEu values, can be interpreted as a reflection of rich water content in magma or a deep magma source, perhaps from thickened lower crust (Defant and Drummond, 1990; Hou et al., 2004). Considering that the Hongshan pluton does not contain much more hydroxyapatite than other three plutons, and

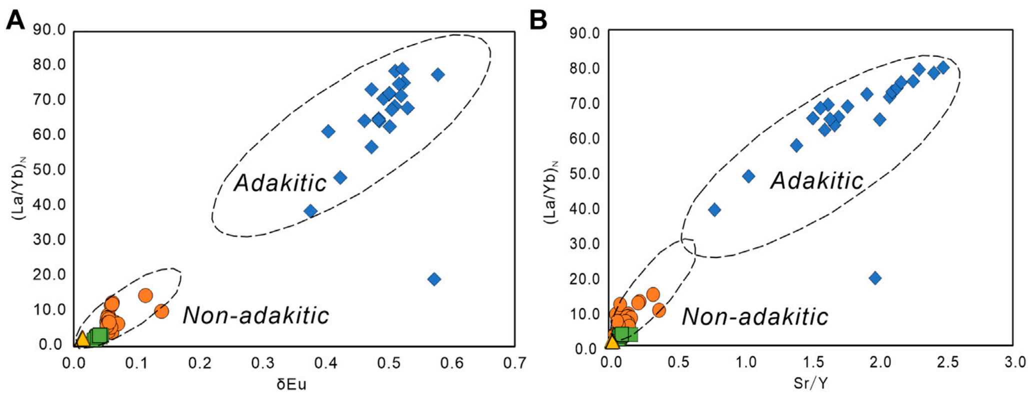

FIGURE 9
(A) Plots of (La/Yb)n versus δEu and **(B)** (La/Yb)n versus Sr/Y in the apatites from the selected four plutons. (based on Pan et al., 2016) (Date are listed in Supplementary Appendix Table SA2).

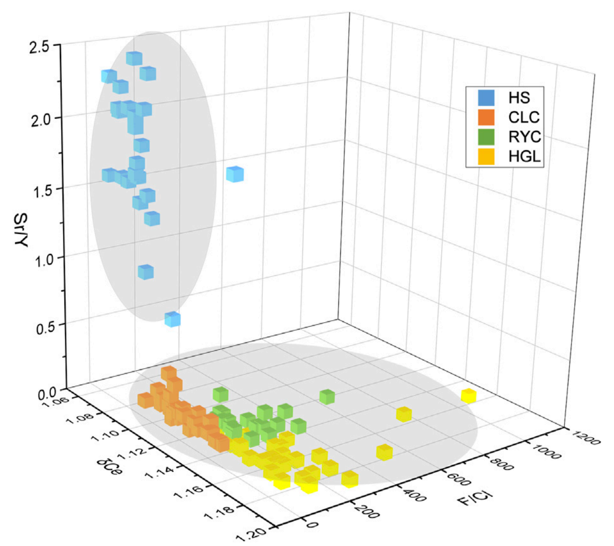

FIGURE 10
Plots of Sr/Y, F/Cl and δCe in apatites from the selected four plutons. (Date are listed in Supplementary Appendix Table SA2).

amphibolite, which is a sign of hydrous magma is widespread in both the Hongshan and Cilincuo plutons, there may have been little difference in the magmatic water content between the adakitic and non-adakitic plutons. Thus, we prefer the second possibility.

The origin of the magma of the Hongshan pluton from thickened lower crust was also suggested by the study of Wang et al. (2014a). Previous studies have proposed that the fractional crystallization of garnet at the depth of the thickened lower crust (>40 km) can segregate an amount of Fe^{2+} from magma and effectively elevate oxygen fugacity of residual magma (Tang et al., 2020). This hypothesis, to some extent, explains our finding that the parental magma of the Hongshan pluton, with a relatively deep origin, was more oxidized than that of the Rongyicuo, Cilincuo, and Hagela plutons with relatively shallow origins.

5.5 Apatite as exploration indicator

Porphyry Cu deposits, as mentioned above, are always associated with oxidized and volatile-rich adakitic magma (Shinohara et al., 1995; Candela and Piccoli, 2005). Therefore, a comprehensive index system that is composed of multiple magmatic information can be used to evaluate the porphyry Cu mineralization potential. Our study shows that apatite δCe values can be indicative of magmatic oxygen fugacity, apatite F/Cl values are a reflection of magmatic volatile components, and apatite Sr/Y values can indicate whether the magma was adakitic. Apatite grains from the Cu-mineralized and non-mineralized rocks we have studied here are clearly different in an index system consisting of apatite δCe, F/Cl and Sr/Y values (Figure 10). Although the applicability of such an index system in evaluating porphyry Cu mineralization potential remains to be studied, it is at least effective for the four plutons investigated here, and may be useful for the exploration of porphyry Cu deposits in the Yidun Terrane in general.

6 Conclusion

(1) Based on apatite δCe values, the parental magma of the Cu-mineralized pluton (Hongshan) was more oxidized than those of the non-mineralized plutons (Cilincuo, Rongyicuo, and Hagela), which is consistent with the calculated magmatic oxygen fugacity using zircon chemical composition and whole-rock Fe^{3+}/Fe^{2+} value.
(2) Based on apatite halogen compositions, the parental magma of the Cu-mineralized pluton (Hongshan) contained more Cl than those of the non-mineralized plutons (Cilincuo, Rongyicuo, and Hagela). The parental magmas of the four plutons were all not highly enriched with S.
(3) The evidently negative $\varepsilon_{Nd}(t)$ values of apatite indicate that the four plutons are the products of partial melting of ancient lower crust mixed with a small amount of mantle-derived components. Furthermore, the adakitic chemical signature of the Cu-mineralzied Hongshan pluton, such as high apatite Sr/Y and δEu values, may be a reflection of a deep magma source (i.e., thickened lower ancient crust).

(4) An index system consisting of apatite δCe, Sr/Y, and F/Cl values can effectively distinguish between the Cu-mineralized and non-mineralized plutons studied.

Data availability statement

The original contributions presented in the study are included in the article/Supplementary Material, further inquiries can be directed to the corresponding author.

Author contributions

QL, L-CP, JY, and L-ZX collected the samples; QL, L-CP, and X-SW designed the experiment; QL carried out the experiment; QL and L-CP analyzed the data. QL wrote the manuscript.

Funding

This study was supported by Guizhou Provincial Science and Technology Projects (QKHJC-ZK[2021] YB211), National key R&D plan (Grant 2022YFC2903303), the National Natural Science Foundation of China (Grant 42173069 and U22A20571), and Frontier project of State Key Laboratory of Deposit Geochemistry, Institute of Geochemistry, Chinese Academy of Sciences.

Acknowledgments

We thank Yan-Wen Tang and Zhi-Hui Dai for their assistance in apatite and zircon trace element analysis by LA-ICP-MS, Wen-Qin Zheng and Xiang Li for their support in apatite chemical analysis by EPMA, You-Wei Chen for his help in apatite Nd isotope analysis by LA-MC-ICP-MS and Shu-Qin Yang and Jing Hu for their assistance in the whole-rock chemical analysis by XRF and ICP-MS.

Conflict of interest

The authors declare that the research was conducted in the absence of any commercial or financial relationships that could be construed as a potential conflict of interest.

The reviewer CL declared a shared affiliation with the authors to the handling editor at the time of review.

Supplementary material

The Supplementary Material for this article can be found online at: https://www.frontiersin.org/articles/10.3389/feart.2023.1185964/full#supplementary-material

References

Boudreau, A. E., and Kruger, F. J. (1990). Variation in the composition of apatite through the Merensky cyclic unit in the Western Bushveld Complex. *Econ. Geol. And Bull. Of Soc. Of Econ. Geol.* 85, 737–745. doi:10.2113/gsecongeo.85.4.737

Bruand, E., Storey, C., and Fowler, M. (2016). An apatite for progress; inclusions in zircon and titanite constrain petrogenesis and provenance. *Geol. (Boulder)* 44, 91–94. doi:10.1130/G37301.1

Candela, P. A., and Piccoli, P. M. (2005). *Magmatic processes in the development of porphyry-type ore systems*. Corner, Virginia: GeoScienceWorld. One Hundredth Anniversary Volume.

Candela, P. A. (1986). Toward a thermodynamic model for the halogens in magmatic systems: An application to melt-vapor-apatite equilibria. *Chem. Geol.* 57, 289–301. doi:10.1016/0009-2541(86)90055-0

Cao, M., Li, G., Qin, K., Seitmuratova, E. Y., and Liu, Y. (2012). Major and trace element characteristics of apatites in granitoids from Central Kazakhstan: Implications for petrogenesis and mineralization. *Resour. Geol.* 62, 63–83. doi:10.1111/j.1751-3928.2011.00180.x

Chappell, B. W. (1999). Aluminium saturation in I- and S-type granites and the characterization of fractionated haplogranites. *Lithos* 46, 535–551. doi:10.1016/S0024-4937(98)00086-3

Chelle-Michou, C., and Chiaradia, M. (2017). Amphibole and apatite insights into the evolution and mass balance of Cl and S in magmas associated with porphyry copper deposits. *Contrib. Mineral. Petrol* 172, 105. doi:10.1007/s00410-017-1417-2

Chen, J., Xu, J., Ren, J., and Huang, X. (2017). Late Triassic E-MORB-like basalts associated with porphyry Cu-deposits in the southern Yidun continental arc, eastern Tibet: Evidence of slab-tear during subduction? *Ore Geol. Rev.* 90, 1054–1062. doi:10.1016/j.oregeorev.2016.12.006

Cooke, D. R. (2014). *Treatise on geochemistry, geochemistry of porphyry deposits*. Berlin, Germany: Researchgate, 357–381.

Creaser, R. A., and Gray, C. M. (1992). Preserved initial in apatite from altered felsic igneous rocks: A case study from the middle proterozoic of south Australia. *Geochim. Cosmochim. Ac.* 56, 2789–2795. doi:10.1016/0016-7037(92)90359-Q

Defant, M. J., and Drummond, M. S. (1990). Derivation of some modern arc magmas by melting of young subducted lithosphere. *Nature* 347, 662–665. doi:10.1038/347662a0

Deng, J., Wang, Q. F., and Li, G. J. (2016). Superimposed orogeny and composite metallogenic system: Case study from the Sanjiang Tethyan belt, SW China. *Acta Petrol. Sin.* 32 (8), 2225–2247.

Deng, J., Wang, Q., Li, G., Li, C., and Wang, C. (2014). Tethys tectonic evolution and its bearing on the distribution of important mineral deposits in the Sanjiang region, SW China. *Gondwana Res.* 26, 419–437. doi:10.1016/j.gr.2013.08.002

Deng, J., Wang, Q., and Li, G. (2017). Tectonic evolution, superimposed orogeny, and composite metallogenic system in China. *Gondwana Res.* 50, 216–266. doi:10.1016/j.gr.2017.02.005

Drake, M. J. (1975). The oxidation state of europium as an indicator of oxygen fugacity. *Geochim. Cosmochim. Ac.* 39, 55–64. doi:10.1016/0016-7037(75)90184-2

Goldoff, B., Webster, J. D., and Harlov, D. E. (2012). Characterization of fluor-chlorapatites by electron probe microanalysis with a focus on time-dependent intensity variation of halogens. *Am. Mineral.* 97, 1103–1115. doi:10.2138/am.2012.3812

Guo, Z., Wilson, M., and Liu, J. (2007). Post-collisional adakites in south Tibet: Products of partial melting of subduction-modified lower crust. *Lithos* 96, 205–224. doi:10.1016/j.lithos.2006.09.011

Harrison, T. M., and Watson, E. B. (1984). The behavior of apatite during crustal anatexis: Equilibrium and kinetic considerations. *Geochim. Cosmochim. Ac.* 48, 1467–1477. doi:10.1016/0016-7037(84)90403-4

Hou, Z. Q., Gao, Y. F., Qu, X. M., Rui, Z. Y., and Mo, X. X. (2004). Origin of adakitic intrusives generated during mid-Miocene east–west extension in southern Tibet. *Earth Planet. Sc. Lett.* 220, 139–155. doi:10.1016/S0012-821X(04)00007-X

Hou, Z. Q., Yang, Z. M., Lu, Y. J., Kemp, A., Zheng, Y. C., Li, Q. Y., et al. (2015). A genetic linkage between subduction- and collision-related porphyry Cu deposits in continental collision zones. *Geology* 43, 247–250. doi:10.1130/G36362.1

Hou, Z., Zaw, K., Pan, G., Mo, X., Xu, Q., Hu, Y., et al. (2007). Sanjiang Tethyan metallogenesis in S.W. China: Tectonic setting, metallogenic epochs and deposit types. *Ore Geol. Rev.* 31, 48–87. doi:10.1016/j.oregeorev.2004.12.007

Hou, Z., Zheng, Y., Zeng, L., Gao, L., Huang, K., Li, W., et al. (2012). Eocene–Oligocene granitoids in southern Tibet: Constraints on crustal anatexis and tectonic evolution of the Himalayan orogen. *Earth Planet. Sc. Lett.* 349-350, 38–52. doi:10.1016/j.epsl.2012.06.030

Huang, M., Bi, X., Richards, J. P., Hu, R., Xu, L., Gao, J., et al. (2019). High water contents of magmas and extensive fluid exsolution during the formation of the Yulong porphyry Cu-Mo deposit, eastern Tibet. *J. Asian Earth Sci.* 176, 168–183. doi:10.1016/j.jseaes.2019.02.008

Imai, A. (2002). Metallogenesis of porphyry Cu deposits of the western luzon arc, Philippines: K-Ar ages, SO3 contents of microphenocrystic apatite and significance of intrusive rocks. *Resour. Geol.* 52, 147–161. doi:10.1111/j.1751-3928.2002.tb00127.x

Isnard, H., Brennetot, R., Caussignac, C., Caussignac, N., and Chartier, F. (2005). Investigations for determination of Gd and Sm isotopic compositions in spent nuclear fuels samples by MC ICPMS. *Int. J. Mass Spectrom.* 246, 66–73. doi:10.1016/j.ijms.2005.08.008

Jeffrey, H. T., and Scott, M. K. (1999). Complex zoning in apatite from the Idaho batholith: A record of magma mixing and intracrystalline trace element diffusion. *Am. Mineral.* 84 (4), 581–595. doi:10.2138/am-1999-0412

Jugo, P. J., Luth, R. W., and Richards, J. P. (2001). *Experimental determination of sulfur solubility in basaltic melts at sulfide vs. Sulfate saturation. Possible implications for ore formation*. Washington, D.C., United States: American Geophysical Union.

Ketcham, R. A. (2015). Technical note: Calculation of stoichiometry from emp data for apatite and other phases with mixing on monovalent anion sites. *Am. Mineral.* 100 (7), 1620–1623. doi:10.2138/am-2015-5171

Konecke, B. A., Fiege, A., Simon, A. C., Linsler, S., and Holtz, F. (2019). An experimental calibration of a sulfur-in-apatite oxybarometer for mafic systems. *Geochim. Cosmochim. Ac.* 265, 242–258. doi:10.1016/j.gca.2019.08.044

Laurent, O., Zeh, A., Gerdes, A., Villaros, A., Gros, K., and Słaby, E. (2017). How do granitoid magmas mix with each other? Insights from textures, trace element and Sr–Nd isotopic composition of apatite and titanite from the matok pluton (south Africa). *Contrib. Mineral. Petr.* 172, 80. doi:10.1007/s00410-017-1398-1

Li, Q., Sun, X., Lu, Y., Wang, F., and Hao, J. (2021). Apatite and zircon compositions for miocene mineralizing and barren intrusions in the gangdese porphyry copper belt of southern tibet: Implication for ore control. *Ore Geol. Rev.* 139, 104474. doi:10.1016/j.oregeorev.2021.104474

Li, W. C. (2010). *Southwest Sanjiang multi-island arc basin collision orogenic metallogenic theory and exploration technology*.

Li, W. C., Yin, G. H., Yu, H. J., Lu, Y. X., and Liu, X. L. (2011). The porphyry metallogenesis of Geza volcanic magmatic arc in NW Yunnan. *Acta Petrol. Sin.* 27 (9), 2541–2552.

Liang, Q., Jing, H., and Gregoire, D. C. (2000). Determination of trace elements in granites by inductively coupled plasma mass spectrometry. *Talanta* 51, 507–513. doi:10.1016/s0039-9140(99)00318-5

Liu, Y., Hu, Z., Gao, S., Günther, D., Xu, J., Gao, C., et al. (2008). *In situ* analysis of major and trace elements of anhydrous minerals by LA-ICP-MS without applying an internal standard. *Chem. Geol.* 257, 34–43. doi:10.1016/j.chemgeo.2008.08.004

Loucks, R. R., Fiorentini, M. L., and Henríquez, G. J. (2020). New magmatic oxybarometer using trace elements in zircon. *J. Petrol.* 61. doi:10.1093/petrology/egaa034

Lu, Y., Campbell McCuaig, T., Li, Z., Jourdan, F., Hart, C. J. R., Hou, Z., et al. (2015). Paleogene post-collisional lamprophyres in Western Yunnan, Western Yangtze Craton: Mantle source and tectonic implications. *Lithos* 233, 139–161. doi:10.1016/j.lithos.2015.02.003

Lu, Y. J., Loucks, R. R., Fiorentini, M., Mccuaig, T. C., and Kobussen, A. (2016). *Zircon compositions as a pathfinder for porphyry Cu ± Mo ± Au deposits*. Corner, Virginia: GeoScienceWorld. Society of Economic Geologists Special Publication No. 19 on Tethyan Tectonics and Metallogeny.

Mao, J., Zhou, Z., Feng, C., Wang, Y., Zhang, C., Peng, H., et al. (2012). A preliminary discussion on the Triassic large-scale mineralization and its dynamic background in China. *Geol. China* 39, 35.

Martin, J. S., and John, H. D. (1998). Sulfur evolution of oxidized arc magmas as recorded in apatite from a porphyry copper batholith. *Geology* 26, 523. doi:10.1130/0091-7613(1998)026<0523:seooam>2.3.co;2

Metcalfe, I. (2011). Tectonic framework and phanerozoic evolution of sundaland. *Gondwana Res.* 19, 3–21. doi:10.1016/j.gr.2010.02.016

Middlemost, E. A. K. (1994). Naming materials in the magma/igneous rock system. *Earth-Sci Rev.* 37, 215–224. doi:10.1016/0012-8252(94)90029-9

Miles, A. J., Graham, C. M., Hawkesworth, C. J., Gillespie, M. R., Hinton, R. W., and Bromiley, G. D. (2014). Apatite: A new redox proxy for silicic magmas? *Geochim. Cosmochim. Ac.* 132, 101–119. doi:10.1016/j.gca.2014.01.040

Morley, C. K. (2012). Late cretaceous–early palaeogene tectonic development of SE asia. *Earth-Sci. Rev.* 115, 37–75. doi:10.1016/j.earscirev.2012.08.002

Mungall, J. E. (2002). Roasting the mantle: Slab melting and the Genesis of major Au and Au-rich Cu deposits. *Geology* 30, 915–918. doi:10.1130/0091-7613(2002)030<0915:RTMSMA>2.0.CO;2

Nathwani, C. L., Loader, M. A., Wilkinson, J. J., Buret, Y., Sievwright, R. H., and Hollings, P. (2020). Multi-stage arc magma evolution recorded by apatite in volcanic rocks. *Geology* 48, 323–327. doi:10.1130/G46998.1

Palma, G., Barra, F., Reich, M., Valencia, V., Simon, A. C., Vervoort, J., et al. (2019). Halogens, trace element concentrations, and sr-nd isotopes in apatite from iron oxide-apatite (ioa) deposits in the chilean iron belt: Evidence for magmatic and hydrothermal stages of mineralization. *Geochim. Cosmochim. Ac* 246, 515–540. doi:10.1016/j.gca.2018.12.019

Pan, L., Hu, R., Wang, X., Bi, X., Zhu, J., Fu, S., et al. (2021). Cu-Mo infertile granite: Insights from the late cretaceous plutons in the Northern Yidun Terrane, eastern Tibetan Plateau. *Ore Geol. Rev.* 139, 104494. doi:10.1016/j.oregeorev.2021.104494

Pan, L., Hu, R., Wang, X., Bi, X., Zhu, J., and Li, C. (2016). Apatite trace element and halogen compositions as petrogenetic-metallogenic indicators: Examples from four granite plutons in the Sanjiang region, SW China. *Lithos* 254-255, 118–130. doi:10.1016/j.lithos.2016.03.010

Parat, F., Holtz, F., and Klügel, A. (2011). S-Rich apatite-hosted glass inclusions in xenoliths from La Palma: Constraints on the volatile partitioning in evolved alkaline magmas. *Contrib. Mineral. Petr.* 162, 463–478. doi:10.1007/s00410-011-0606-7

Pearce, J. (1996). Sources and settings of granitic rocks. *Episodes* 19, 120–125.

Peng, G. Y., Luhr, J. F., and McGee, J. J. (1997). Factors controlling sulfur concentrations in volcanic apatite. *Am. Mineral.* 82, 1210–1224. doi:10.2138/am-1997-11-1217

Peng, H.-J. (2014). *Metallogeny of the hongniu-hongshan porphyry-skarn copper deposit and the porphyry-skarn metallogenic system of the Yidun island Arc,Yunnan,SW China*. Beijing, Xicheng: Chinese Academy of Geological Sciences. A Dissertation Submitted to Chinese Academy of Geological Sciences for the Doctoral Degree.

Piccoli, P. M., and Candela, P. A. (2002). Apatite in igneous systems. *Rev. Mineralogy Geochem.* 48, 255–292. doi:10.2138/rmg.2002.48.6

Piccoli, P. (1989). Tectonic discrimination of granitoids. *GSA Bull. GSA Bull.* 101 (5), 635–643. doi:10.1130/0016-7606(1989)101<0635:TDOG>2.3.CO;2

Qing, F., Wang, J., Chusi, L., Gong, J., and Li, L. (2014). The boundary between the Simao and Yangtze blocks and their locations in Gondwana and Rodinia: Constraints from detrital and inherited zircons. *Gondwana Res.* 26, 438–448. doi:10.1016/j.gr.2013.10.002

Richards, J. P. (2011). High Sr/Y arc magmas and porphyry Cu Mo Au deposits: Just add water. *Econ. Geol.* 106, 1075–1081. doi:10.2113/econgeo.106.7.1075

Richards, J. P., López, G. P., Zhu, J., Locock, A. J., and Mumin, A. H. (2017). Contrasting tectonic settings and sulfur contents of magmas associated with cretaceous porphyry Cu ± Mo ± Au and intrusion-related iron oxide Cu-Au deposits in northern Chile. *Econ. Geol.* 112, 295–318. doi:10.2113/econgeo.112.2.295

Richards, J. P. (2003). Tectono-magmatic precursors for porphyry Cu-(Mo-Au) deposit formation. *Econ. Geol. And Bull. Of Soc. Of Econ. Geol.* 98, 1515–1533. doi:10.2113/gsecongeo.98.8.1515

Richards, J. P. (2015). The oxidation state, and sulfur and Cu contents of arc magmas: Implications for metallogeny. *Lithos* 233, 27–45. doi:10.1016/j.lithos.2014.12.011

Schwartz, M. O., Rajah, S. S., Askury, A. K., Putthapiban, P., and Djaswadi, S. (1995). The Southeast Asian tin belt. *Earth-Sci. Rev.* 38, 95–293. doi:10.1016/0012-8252(95)00004-T

Sha, L., and Chappell, B. W. (1999). Apatite chemical composition, determined by electron microprobe and laser-ablation inductively coupled plasma mass spectrometry, as a probe into granite petrogenesis. *Geochim. Cosmochim. Ac.* 63, 3861–3881. doi:10.1016/S0016-7037(99)00210-0

Shinohara, H., Kazahaya, K., and Lowenstern, J. B. (1995). Volatile transport in a convecting magma column: Implications for porphyry Mo mineralization. *Geology* 23, 1091. doi:10.1130/0091-7613(1995)023<1091:vtiacm>2.3.co;2

Sillitoe, R. H. (2010). Porphyry copper systems. *Econ. Geol.* 105, 3–41. doi:10.2113/gsecongeo.105.1.3

Stormer, J. C., Pierson, M. L., and Tacker, R. C. (1993). Variation of F and Cl X-ray intensity due to anisotropic diffusion in apatite during electron. *Am. Mineral.* 78, 641.

Streck, M. J., and Dilles, J. H. (1998). Sulfur evolution of oxidized arc magmas as recorded in apatite from a porphyry copper batholith. *Geology* 26, 523–526. doi:10.1130/0091-7613(1998)026<0523:SEOOAM>2.3.CO;2

Sun, S.-s., and McDonough, W. F. (1989). Chemical and isotopic systematics of oceanic basalts: Implications for mantle composition and processes. *Geol. Soc. Lond. Spec. Publ.* 42, 313–345. doi:10.1144/GSL.SP.1989.042.01.19

Sun, S., Yang, X., Wang, G., Sun, W., Zhang, H., Li, C., et al. (2019). *In situ* elemental and Sr-O isotopic studies on apatite from the Xu-Huai intrusion at the southern margin of the North China Craton: Implications for petrogenesis and metallogeny. *Chem. Geol.* 510, 200–214. doi:10.1016/j.chemgeo.2019.02.010

Tang, M., Lee, C. A., Ji, W. Q., Wang, R., and Costin, G. (2020). Crustal thickening and endogenic oxidation of magmatic sulfur. *Sci. Adv.* 6, eaba6342. doi:10.1126/sciadv.aba6342

Tsuboi, M., and Suzuki, K. (2003). Heterogeneity of initial 87 Sr/86 Sr ratios within a single pluton: Evidence from apatite strontium isotopic study. *Chem. Geol.* 199, 189–197. doi:10.1016/S0009-2541(03)00085-8

Tsuboi, M. (2005). The use of apatite as a record of initial 87Sr/86Sr ratios and indicator of magma processes in the Inagawa pluton, Ryoke belt, Japan. *Chem. Geol.* 221, 157–169. doi:10.1016/j.chemgeo.2005.05.001

Wang, P., Dong, G., Zhao, G., Han, Y., and Li, Y. (2018). Petrogenesis of the Pulang porphyry complex, southwestern China: Implications for porphyry copper metallogenesis and subduction of the Paleo-Tethys Oceanic lithosphere. *Lithos* 304-307, 280–297. doi:10.1016/j.lithos.2018.02.009

Wang, R., Luo, C., Xia, W., Sun, Y., Liu, B., and Zhang, J. (2021). Research progress on the Genesis of high-water and high-oxygen fugacity magma in the Gangdise post-collision porphyry metallogenic belt. *Mineral. rock Geochem. Rep.* 40, 1061–1077. +997.

Wang, R., Richards, J. P., Hou, Z. Q., Yang, Z. M., and DuFrane, S. A. (2014). Increased magmatic water content--the key to oligo-miocene porphyry Cu-Mo Au formation in the eastern gangdese belt, tibet. *Econ. Geol.* 109, 1315–1339. doi:10.2113/econgeo.109.5.1315

Wang, R., Weinberg, R. F., Collins, W. J., Richards, J. P., and Zhu, D. C. (2018). Origin of postcollisional magmas and formation of porphyry Cu deposits in southern Tibet. *Earth-Sci. Rev.* 181, 122–143. doi:10.1016/j.earscirev.2018.02.019

Wang, R., Zhu, D., Wang, Q., Hou, Z., Yang, Z., Zhao, Z., et al. (2020). Porphyry mineralization in the Tethyan orogen. *Sci. China Earth Sci.* 63, 2042–2067. doi:10.1007/s11430-019-9609-0

Wang, X., Bi, X., Leng, C., Zhong, H., Tang, H., Chen, Y., et al. (2014a). Geochronology and geochemistry of Late Cretaceous igneous intrusions and Mo–Cu–(W) mineralization in the southern Yidun Arc, SW China: Implications for metallogenesis and geodynamic setting. *Ore Geol. Rev.* 61, 73–95. doi:10.1016/j.oregeorev.2014.01.006

Wang, X., Hu, R., Bi, X., Leng, C., Pan, L., Zhu, J., et al. (2014b). Petrogenesis of late cretaceous I-type granites in the southern Yidun terrane: New constraints on the late mesozoic tectonic evolution of the eastern Tibetan plateau. *Lithos* 208-209, 202–219. doi:10.1016/j.lithos.2014.08.016

Wang, X., Jia, J., and Wang, Y. (2011). Degradation of c.i. Reactive red 2 through photocatalysis coupled with water jet cavitation. *J. Hazard Mater* 185, 315–321. doi:10.1016/j.jhazmat.2010.09.036

Webster, J. D. (2004). The exsolution of magmatic hydrosaline chloride liquids. *Chem. Geol.* 210, 33–48. doi:10.1016/j.chemgeo.2004.06.003

Wen, G., Zhou, R., Li, J., Chang, J., Hu, H., Yan, D., et al. (2020). Skarn metallogeny through zircon record: An example from the daye cu-au-fe-mo district, eastern China. *Lithos* 378-379, 105807. doi:10.1016/j.lithos.2020.105807

Whalen, J. B., Currie, K. L., and Chappell, B. W. (1987). A-type granites - geochemical characteristics, discrimination and petrogenesis. *Contrib. Mineral. Petr* 95, 407–419. doi:10.1007/BF00402202

Xing, K., Shu, Q., and Lentz, D. R. (2021). Constraints on the formation of the giant daheishan porphyry Mo deposit (NE China) from whole-rock and accessory mineral geochemistry. *J. Petrol.* 62. doi:10.1093/petrology/egab018

Xing, K., Shu, Q., Lentz, D. R., and Wang, F. (2020). Zircon and apatite geochemical constraints on the formation of the Huojihe porphyry Mo deposit in the Lesser Xing'an Range, NE China. *Am. Mineral.* 105, 382–396.

Yang, Y., Wu, F., Yang, J., Chew, D. M., Xie, L., Chu, Z., et al. (2014). Sr and Nd isotopic compositions of apatite reference materials used in U–Th–Pb geochronology. *Chem. Geol.* 385, 35–55. doi:10.1016/j.chemgeo.2014.07.012

Zhang, K., Zhang, Y., Tang, X., and Xia, B. (2012). Late Mesozoic tectonic evolution and growth of the Tibetan plateau prior to the Indo-Asian collision. *Earth-Sci. Rev.* 114, 236–249. doi:10.1016/j.earscirev.2012.06.001

Zhang, W., Shao, J., Wang, R., Xu, X., Che, X., and Yang, Y. (2011). Sr-rich apatite from the Dangzishan leucitite-ijolite xenoliths (Heilongjiang Province): Mineralogy and mantle-fluid metasomatism. *Chin. Sci. Bull.* 56, 53–63. doi:10.1007/s11434-010-4228-7

Zhao, Z. (2010). Trace element geochemistry of accessory minerals and its applications in petrogenesis and metallogenesis. *Earth Sci. Front.* 17 (1), 267–286.

Zhou, R., Wen, G., Li, J., Cao, K., Wei, K., Cai, H., et al. (2022b). Petrogenesis and metal fertility of yinzu pluton in the daye district, eastern China: Insights from whole-rock and mineral (zircon, apatite and amphibolite) geochemistry. *Lithos* 432-433, 106898. doi:10.1016/j.lithos.2022.106898

Zhou, R., Wen, G., Li, J., Jiang, S., Hu, H., Deng, X., et al. (2022a). Apatite chemistry as a petrogenetic–metallogenic indicator for skarn ore-related granitoids: An example from the daye fe–cu–(au–mo–w) district, eastern China. *Contrib. Mineral. Petr* 177, 23. doi:10.1007/s00410-022-01890-0

Zhu, D., Zhao, Z., Niu, Y., Mo, X., Chung, S., Hou, Z., et al. (2011). The Lhasa Terrane: Record of a microcontinent and its histories of drift and growth. *Earth Planet. Sc. Lett.* 301, 241–255. doi:10.1016/j.epsl.2010.11.005

Zhu, J., Richards, J. P., Rees, C., Creaser, R., DuFrane, S. A., Locock, A., et al. (2018). Elevated magmatic sulfur and chlorine contents in ore-forming magmas at the red chris porphyry Cu-Au deposit, northern British columbia, Canada. *Econ. Geol.* 113, 1047–1075. doi:10.5382/econgeo.2018.4581